Sentinel-1 based analysis of the Pakistan Flood in 2022

Florian Roth[1], Bernhard Bauer-Marschallinger[1], Mark Edwin Tupas[1, 2], Christoph Reimer[3],
Peter Salamon[4], and Wolfgang Wagner[1]

[1]Department of Geodesy and Geoinformation, TU Wien, Vienna, Austria
[2]Department of Geodetic Engineering, University of the Philippines Diliman, Quezon City, Philippines
[3]EODC Earth Observation Data Centre for Water Resources Monitoring GmbH, Vienna, Austria
[4]European Commission, Joint Research Centre, Via E. Fermi 2749, 21027 Ispra, Italy

Correspondence: Florian Roth (florian.roth@geo.tuwien.ac.at)

Abstract. In August and September 2022, Pakistan was hit by a severe flood and millions of people were impacted. The
Sentinel-1 based flood mapping algorithm developed by Technische Universität Wien (TU Wien) for the Copernicus Emergency Management Service (CEMS) global flood monitoring (GFM) component was used to document the propagation of the
flood from August 10 to September 23, 2022. The results were evaluated using the flood maps from the CEMS rapid mapping
component. Overall, the algorithm performs reasonably with a critical success index of up to 80 %, while the detected differences are traced back to different sensors used for the flood mapping. Over the 6 weeks timespan an area of 30,492 km^2 was
observed to be flooded at least once, and the maximum extent was found to be present on August 30.

1 Introduction

Pakistan is a flood prone country due to its uneven topography and heavy rainfall during the monsoon season (Sayama et al.,
2012; Qasim et al., 2015; Sajjad et al., 2020). One outstanding event happened in 2010 and affected about 14 million people
(Gaurav et al., 2011). Starting from mid-June 2022 Pakistan was hit by the country's worst flooding in a decade and tens of
thousands of square kilometres were inundated (NASA Earth Observatory).

As the 2022 flood destroyed many roads and other infrastructure and the extent of the inundated area covered an extremely
large area, satellite data was the only way of providing large scale information of the affected area to local authorities. Among
others, the Copernicus Earth Observation programme gives access to systematic observations of the Earth's surface, providing
crucial information on natural disasters. Especially, the C-band synthetic aperture radar (SAR) mission Sentinel-1 provides
cloud independent all-day imagery with unprecedented spatio-temporal sampling, enabling the mapping of flooded areas.
To retrieve the flooded areas from the satellite data, the Copernicus Emergency Management Service (CEMS) offers two
components: The rapid mapping service and the global flood monitoring (GFM) (Salamon et al., 2021) service. While the rapid
mapping service works on demand of an authorized user and makes use of many different satellite missions, the GFM fully
relies on SAR data and provides results for each incoming scene in near-real-time (NRT). The service utilizes three independent
flood mapping algorithms and provides an ensemble result. One of the algorithms has been developed by Technische Universität
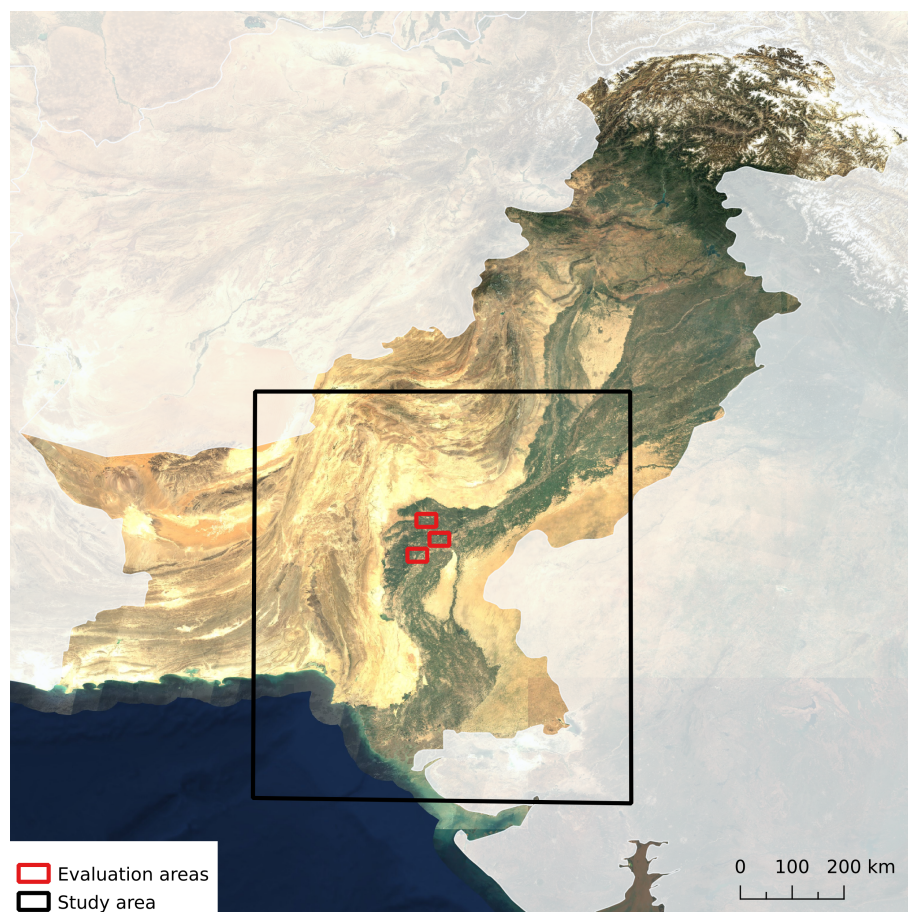
Figure 1. Study and evaluation areas over Pakistan. Background: https://s2maps.eu Sentinel-2 cloudless 2021 by EOX IT Services GmbH is licensed under a Creative Commons Attribution-NonCommercial-ShareAlike 4.0 International License.

Wien (TU Wien) (Bauer-Marschallinger et al., 2022) and its results for the flood in Pakistan 2022 are shown and evaluated in this study.

In detail, the NRT results of the TU Wien algorithm are collected in a dedicated dataset of flooded extent maps in Pakistan from August 10 to September 23, 2022. Based on this dataset, we present our estimation of the affected area and the progress of the flood. To evaluate the quality of the presented dataset, it is compared to results of the rapid mapping service. The study aims to give a quick estimate on the flood's impact and for supporting further studies by sharing our results and insights with the scientific community.
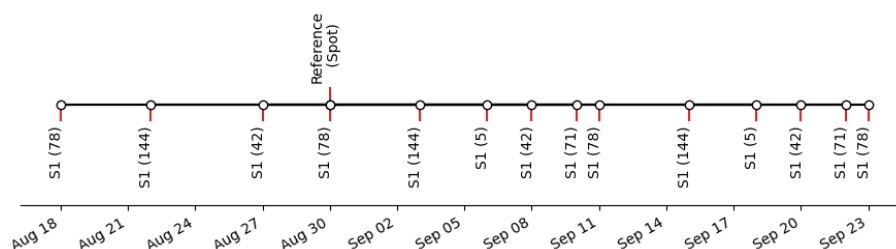
Figure 2. Timeline of Sentinel-1 overpasses and their respective relative orbits in parentheses. Additionally, the ~~time~~ of the overpass of Spot is shown, which is used for the production of the used reference data.

2 Methodology and study area

The provided dataset deals with the most affected parts of Pakistan covering the southern provinces *Punchab*, *Sindh*, and *Balochistan* (details can be seen in Figure 1). In the selected timeframe (2022/08/10 to 2022/09/23) the area was captured by 14 Sentinel-1 overpasses and was observed from 5 different relative orbits (see Figure 2 for more details). The flood extent of 35 all of these Sentinel-1 observations is retrieved by our TU Wien flood mapping algorithm.

Calm open water surfaces appear flat when being hit by C-band SAR radiation, and the radiation is scattered away from the satellite's sensor. Consequently, the received energy (measured as backscatter) is low and shows high contrast to general land surfaces. Generally, the underlying principle of the SAR-based flood mapping methods is to identify low backscatter measurements where land is expected under normal conditions. For this purpose, the TU Wien flood mapping algorithm 40 (Bauer-Marschallinger et al., 2022) utilizes backscatter signatures for flooded and non-flooded conditions retrieved from historic Sentinel-1 measurements. An incoming Sentinel-1 observation is compared to both signatures on a pixel basis, and the most probable condition is selected using the Bayes decision rule. As the general intention of the algorithm is the use in NRT applications, the class signatures are based on statistical backscatter models defined by a limited number of predefined parameters. This setup allows for efficient access to multiple years of backscatter characteristics, but one needs to take into account 45 the limitations of the applied models. Consequently, pixels where no informed decision is possible are masked automatically due to inconclusive information in the given observations and statistical parameters.

Flood mapping based on SAR data suffers from certain limitations, and the GFM service deals with these by applying a dedicated exclusion mask onto the flood mapping result (details are given in Global Flood Monitoring). The mask takes into account areas where Sentinel-1 has no sensitivity (e.g. dense vegetation, urban areas), areas of permanent low backscatter (e.g. 50 tarmac surfaces, deserts), areas of topographic distortions (e.g. mountains) and radar shadows. Following this approach, the GFM exclusion mask is applied onto the TU Wien results as well.

Finally, the flood classification of an incoming Sentinel-1 observation can be represented by a binary map, showing detected flooded areas. Pixels masked by the algorithm or the exclusion mask are set to no data. The impact and progress of the flood is estimated by exploiting the resulting time-series of binary flood extent maps. The flood frequency is ~~known~~ as the ratio of 55 flood detections and number of observations per pixel (Pekel et al., 2016; Pelich et al., 2017). This statistical value allows for
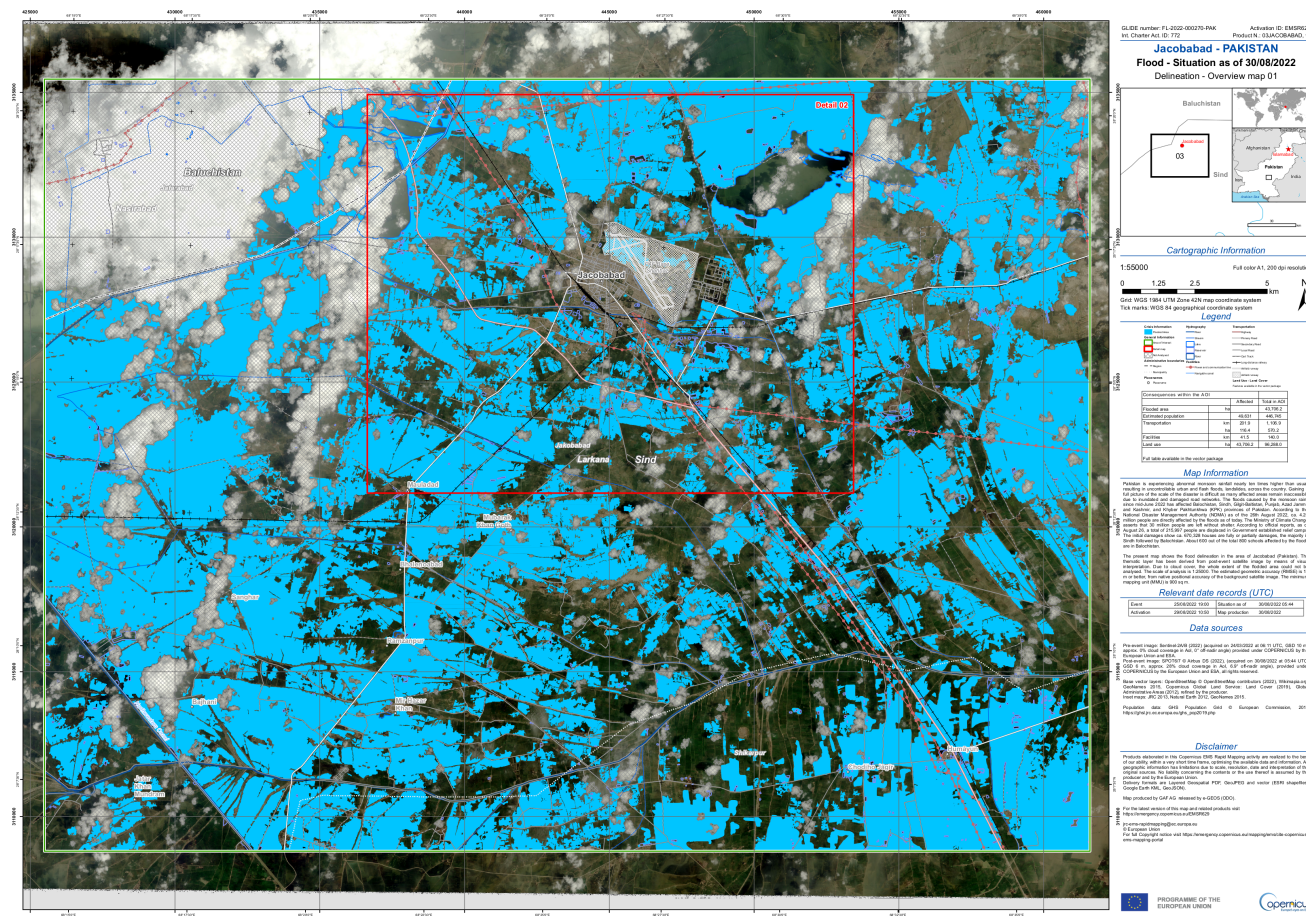
Figure 3. Exemplary CEMS rapid mapping service delineation product for Jacobabad. Copernicus Emergency Management Service (© 2022 European Union), [EMSR629] Jacobabad: Delineation Map, version 2

estimating the area flooded at least once during a time period and is often used to show the flood impact of a certain event (Wang, 2004; Hoque et al., 2011). Additionally, pixels can be identified, which are flooded during the whole time of the study. The progress of the flood is derived by analysing the results of one relative orbit covering the study area best. To present the flood's progress based on multiple orbits, the time of the first flood detection of each pixel is shown in a dedicated layer.

60 **3 Evaluation**

To evaluate the performance of the TU Wien flood mapping algorithm, its results are compared to the results of the CEMS rapid mapping component. As described by Wania et al. (2021), the CEMS rapid mapping service provides crisis information on-demand and handles map requests, production and dissemination. In the context of flood mapping, the delineation products

Table 1. Used reference datasets and the corresponding Sentinel-1 acquisition times.

AOI	Sensor (reference)	Acquisition time (reference)	Acquisition time (Sentinel-1)
Larkana	SPOT-6-7	2022/08/30 05:44:37	2022/08/30 01:25:51
Shikarpur	SPOT-6-7	2022/08/30 05:45:30	2022/08/30 01:25:51
Jacobabad	SPOT-6-7	2022/08/30 05:44:37	2022/08/30 01:25:51

(example given in Figure 3) are of particular interest as they include the observed flood extent of a given time. The inundated
65 areas are classified by using a semi-automatic approach, which includes manual expertise and automatic classification. The
vector-based delineation products are converted to raster format, to allow a pixel-based comparison to the TU Wien results.
Furthermore, permanent water bodies and cloud-covered areas are retrieved from the delineation products and excluded from
the validation, as well as areas masked by the TU Wien algorithm. Resulting differences of TU Wien results and reference data
are summarized in confusion maps, and tables from where the common validation metrics were calculated. These include the
70 user's and producer's accuracy (UA and PA) as well as the critical success index (CSI).

By the time of writing, the rapid mapping service records two activations related to the 2022 flood in Pakistan ([EMSR629]
and [EMSR631]), which include four areas of interest (AOI): *Jacobabad*, *Larkana*, *Shikarpur* and *Sanghar*. Since the satellite
acquisition of only three AOI are within two days of a Sentinel-1 acquisition of the same region (listed in Table 1), only these
are incorporated in the evaluation of this study. It can be seen that the AOI cover only small fractions of the whole study area.
75 Due to the lack of comparable large-scale reference data, the evaluation is limited to these samples. For all AOI, the high-
resolution optical satellite system Spot was used to detect flooded areas, and the acquisitions were within hours of the closest
Sentinel-1 acquisition. Consequently, the comparison of TU Wien and the rapid mapping service results are not only influenced
by the difference in methodology but also by the used sensor and slightly by the time difference between the acquisitions.

4 Results and discussion

80 ### 4.1 Evaluation results

The result of the evaluation is shown in Table 2. Generally, the algorithm performed reasonably taken into account the differ-
ences in the sensor and acquisition time. While the performance is best in *Larkana*, the results in *Jacobabad* and *Shikarpur*
show more under- and overestimation. Figures 4 to 6 show more details about the detected differences by presenting areas
of over- and underestimation as well as areas of agreement. Additionally, the figures contain the backscatter under normal
85 conditions as expected from the non flood statistical model, utilized by the TU Wien algorithm, and the investigated Sentinel-1
observation showing the flood extent during the acquisition time.

The detected underestimation in the *Shikarpur* AOI can be traced back to differences in the used sensor for flood mapping.
As visible in the Sentinel-1 observation (Figure 6 (b)), the low backscatter areas match the flood classification well, while

5

Table 2. Validation measures for each AOI of the CEMS rapid mapping service.

| AOI	UA [%]	PA [%]	CSI [%]
Larkana	94.5	84.2	80.2
Shikarpur	97.1	68.6	67.3
Jacobabad	82.1	86.9	73.0
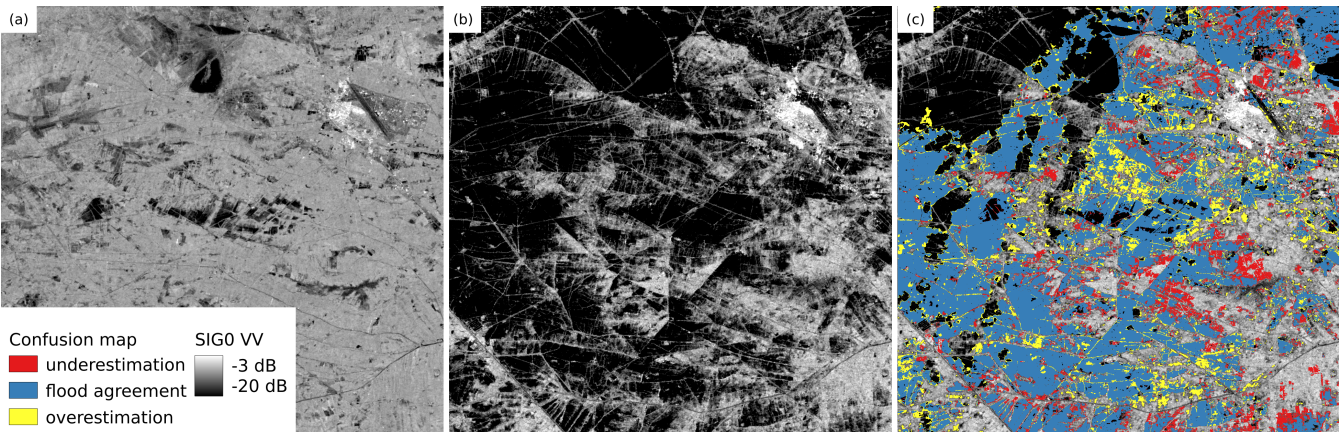
Figure 4. Evaluation for AOI Jacobabad (reference: Copernicus Emergency Management Service (© 2022 European Union), [EMSR629] Jacobabad: Delineation Map, version 1). (a) Expected backscatter from the harmonic model (b) SIG0 VV observation from 2022/08/30 (c) Confusion map

the pixels classified as flood by the rapid mapping service result show a higher backscatter. One can assume the presence of vegetation covering the water surface. Pierdicca et al. (2017) and Landuyt et al. (2020) emphasized the requirement of two SAR polarizations (VV and VH) to allow a detection of flooded vegetation. Furthermore, they showed the potential of the use of optical data to benefit the retrieval. It can be assumed that the flood mapping based on optical data provided by Spot is able to detect this inundation, while the Sentinel-1 based approach missed it. Alternatively, the time difference between Sentinel-1 and Spot over these areas might have result in the observed differences. Similar differences can be also seen for the other two AOI (Figure 4 and 5).

The confusion map of the *Jacobabad* AOI (Figure 4 (c)) shows a large area of low backscatter in the northwest part of the map, which is not participating in the validation. This can be explained by the inability of optical sensors to penetrate clouds. While the SAR-based approach provides details on the flood extent of this area, the optical approach needs to be masked due to cloud coverage. Comparing the confusion map and the original optical image (visible in Figure 3), one can assume that cloud shadows prevent the flood detection additionally and are shown as overestimation in the confusion map. However, water-like low backscatter over vegetation or the difference in acquisition time of the two sensors might explain the overestimation as well.
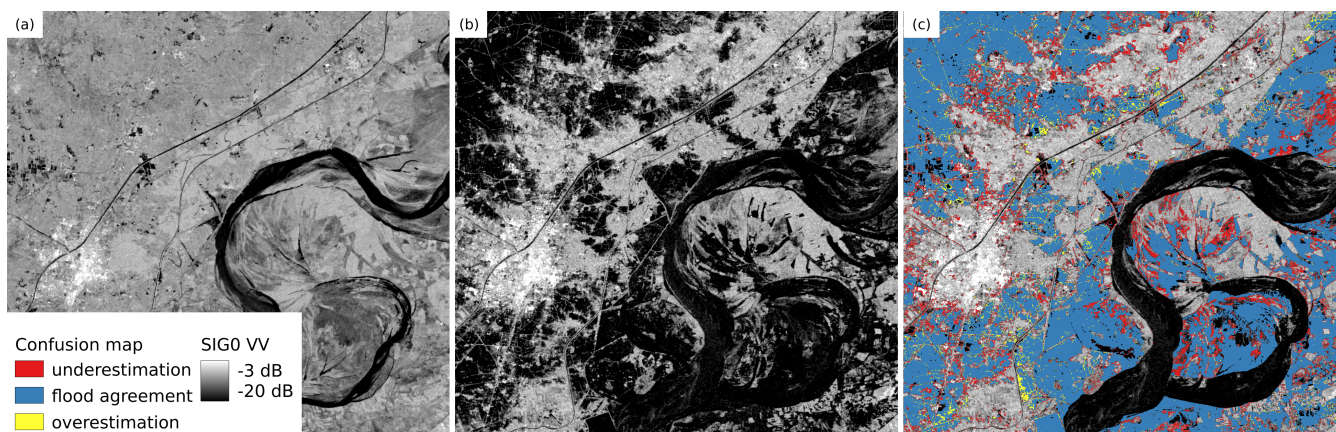
Figure 5. Evaluation for AOI Larkana (reference: Copernicus Emergency Management Service (© 2022 European Union), [EMSR629] Larkana: Delineation Map, version 2). (a) Expected backscatter from the harmonic model (b) SIG0 VV observation from 2022/08/30 (c) Confusion map
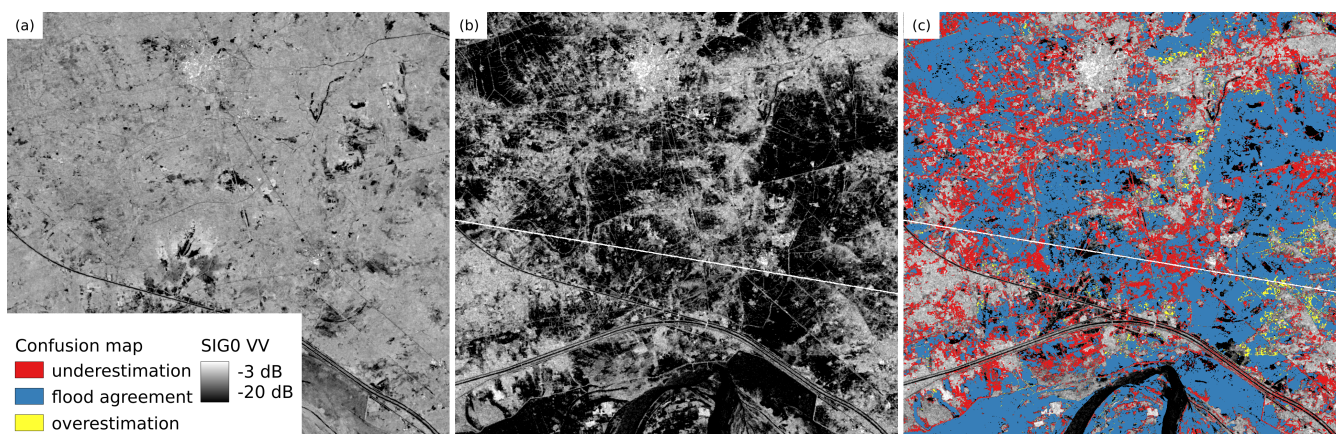

Figure 6. Evaluation for AOI Shikarpur (reference: Copernicus Emergency Management Service (© 2022 European Union), [EMSR629] Shikarpur: Delineation Map, version 1). (a) Expected backscatter from the harmonic model (b) SIG0 VV observation from 2022/08/30 (c) Confusion map

4.2 Statistical layers

Overall, the area observed by Sentinel-1 and not masked by the algorithm accounts for 205,287 km^2. The flood mapping results of 14 timestamps are summarized into specific statistical layers showing the flood impact and progress.

Satellite observations capture an area at distinct times and, especially in case of large scale areas, there is no guarantee of a complete coverage at the same time. In case of the flood in Pakistan, the descending relative orbit 78 of Sentinel-1 covers the majority of the study area at a single overpass. Consequently, this relative orbit is well suited for analysing the temporal

105

7
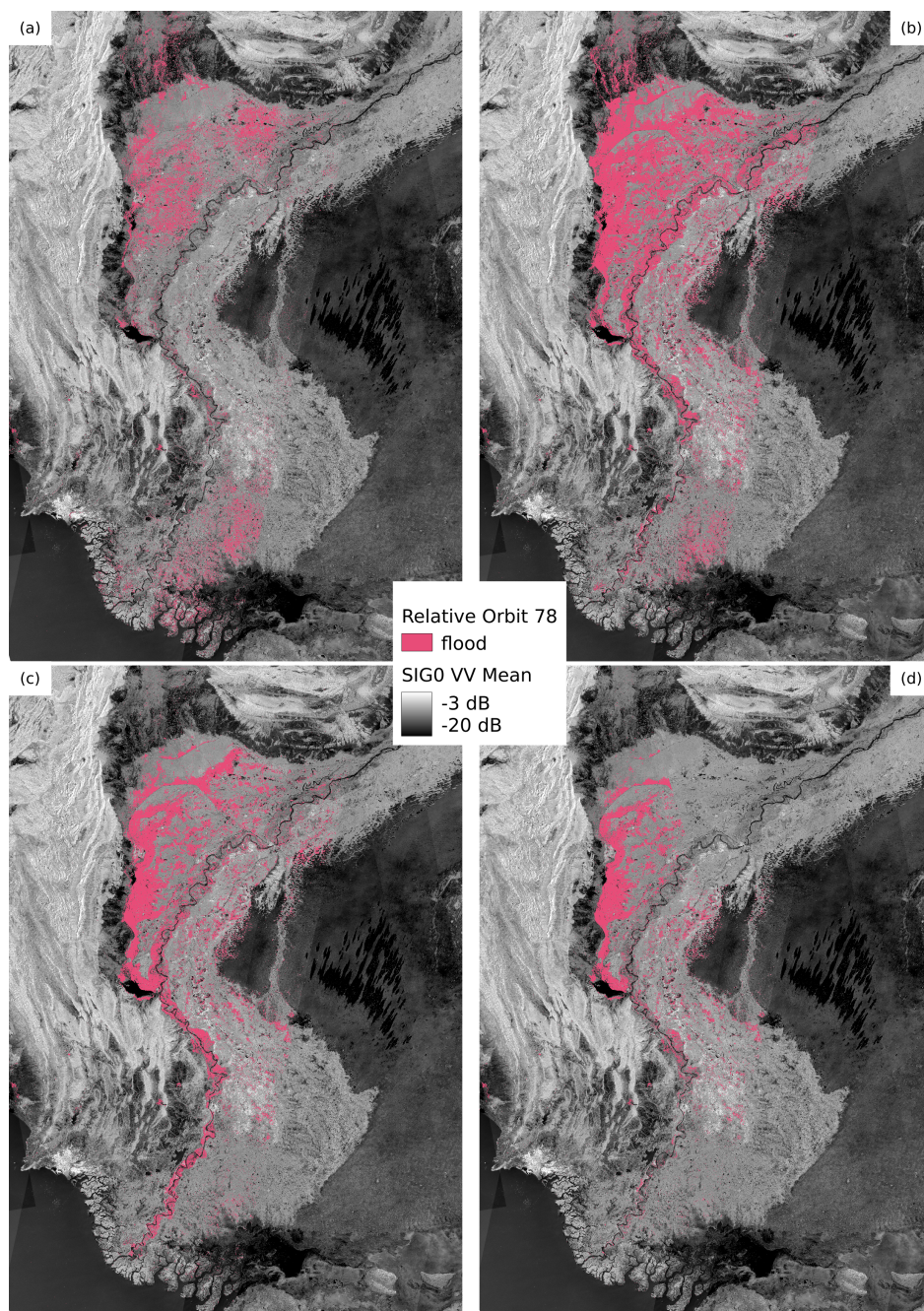
Figure 7. Progress of the flood as seen from Sentinel-1 relative orbit 78 on top of the Sentinel-1 SIG0 VV mean image (2019-2020). (a) 2022/08/18 with a flooded area of 8,448 km^2 (b) 2022/08/30 with a flooded area of 18,047 km^2 (c) 2022/09/11 with a flooded area of 12,013 km^2 (d) 2022/09/23 with a flooded area of 6,331 km^2.
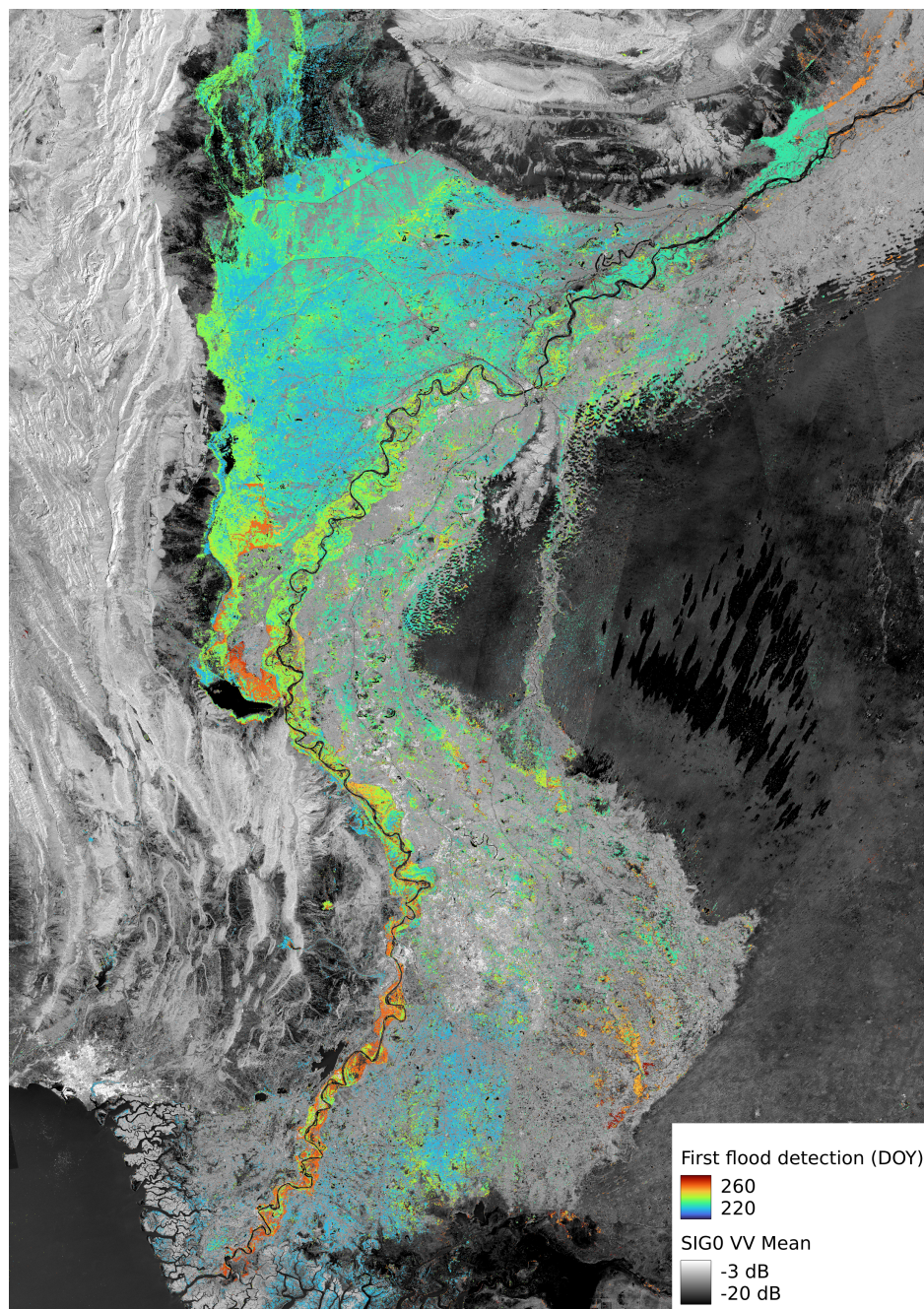
Figure 8. Flood affected area colour-coded with the time of the first flood detection as day-of-year (DOY) on top of the Sentinel-1 SIG0 VV mean image (2019-2020).
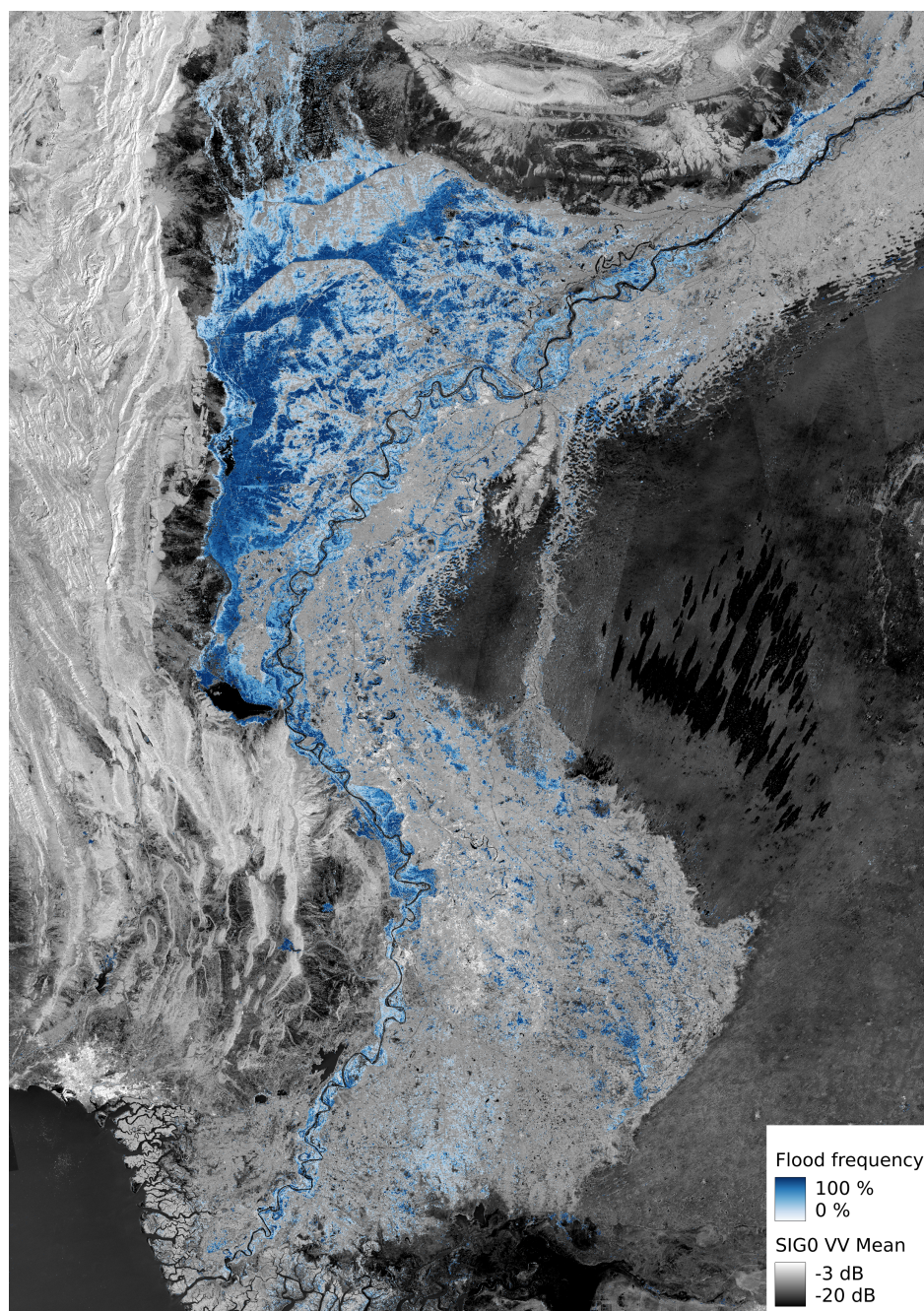
Figure 9. Flood frequency of the study's time period (2022/08/10 to 2022/09/23) on top of Sentinel-1 SIG0 VV mean image (2019-2020).

progress of the flood event. The results of the four overpasses during the study's time period are shown in Figure 7. Starting from August 18 the flood surface increased until it reached its maximum at August 30. The following-up observation of this

110

relative orbit on August 11 show a decrease of the flood surface in the north, while the flood increased in the south next to the river. On August 23 the flood decreased in the north and the south. Due to the discrete information provided by satellite data, the maximum of the flood can not be determined precisely, but a well-informed estimate can be given.

A similar progress can be observed in Figure 8, which presents the time of a pixel being first flooded as day-of-year (DOY).

115 A unique feature of satellite-derived products is the possibility to perform this kind of spatio-temporal analysis and gather large-scale information about an emergency situation. The flood started in the blue areas mainly in the northern part and continued towards the south, where more orange areas are visible. Here, all available relative orbits are combined, which allows for an analysis over more timestamps. However, some artefacts related to the multi-orbit approach can be seen in the figure. Since the whole area is not always covered by one overpass, Figure 8 shows some discontinuous locations without any hydrological

120 reason. This issue can be seen in the northeast, where the flood coloured in green is captured earlier compared to the close by orange area and a linear cut is visible.

Figure 9 shows the flood frequency for the study's time period (2022/08/10 to 2022/09/23) as percentage. As the flood frequency is nearly independent of the relative orbits covering each pixel, the orbit effects of Figure 8 are not visible. The area, which is consistently flooded for the study's time period, corresponds to 5,479 km^2. Analysing the pixels classified as

125 flood at least once during the time period results in an overall affected area of 30,492 km^2, which is close to the total area of Belgium. The vast majority of the flooded area is located close to the river *Indus*. This matches reports of previous flood events in Pakistan (Gaurav et al., 2011), where the extreme run-off of the river caused the flood in the souther parts of the country. Furthermore, the evaluation (see Section 4.1) is performed within close distance to the river as well and confirms the estimated flood extent. In the background of Figure 9 the average backscatter of the years 2019 and 2020 is presented. The area next

130 to the river *Indus* is dominated by crop land, but includes tree cover and built-up areas as well. Considered together, this area shows a higher backscatter within the mean image. In the east of the map, the desert *Thar* is visible, which partly features a low water-like backscatter. While the exclusion mask removes the majority of low backscatter areas, yearly rotating crop types or varying growing seasons impede the flood mapping over agricultural areas. Especially the small individual flood areas need to be treated cautiously when being used in further studies.

135 ## 5 Conclusions

This study shows the potential of providing information in NRT on large scale flood events, and the retrieved data allow for an estimate of the affected area and the progress of the event. Overall, an area of 30,492 km^2 has been observed to be affected by flood, which corresponds to about 15 % of the observed area in this study. ~~Analysing the relative orbit 78,~~ the flood extent increased from the beginning of the timespan on August 18, increased until August 30 and decreased afterwards. The flood

140 extent visible from relative orbit 78 at August 30 reached 18,047 km^2, while at the end of the time period on September 23 there is still 6,331 km^2 flooded.

It can be assumed that this kind of information is especially valuable in situations where ground-based methods are unavailable due to the destruction of infrastructure. Furthermore, Sentinel-1 has proven to provide reasonable coverage over the study

145 area, although the mission is more focussed on Europe. This was achieved after the failure of Sentinel-1B, which left a single satellite in orbit and ~~reduced~~ the temporal resolution ~~significantly~~. Nevertheless, satellite data provides discrete information both in spatial and temporal domain and the impact or the precise progress of an event cannot be fully represented.

The performed evaluation of the produced result was only applied on three comparatively small sites due to the limited availability of reference data. The resulting differences between the TU Wien results and the reference data are found to be mostly related to the different sensor used for producing the flood extent maps. Consequently, the algorithm performed

150 satisfactorily for the given evaluation sites. However, the method faces some known challenges and the lack of large-scale reference data does not allow a verification of all the potentially affected areas. In detail, this refers to land cover types like vegetation or desert.

~~One of the group's upcoming studies~~ will focus on the evaluation of the algorithm in more detail by analysing eighteen globally distributed events ~~(Roth et al., in preparation)~~. Furthermore, the challenges of some land cover types will be tackled

155 by dedicated studies to gain more trust in the flood mapping results over these areas. The upcoming start of Sentinel-1C will again result in a complete constellation of two Sentinel-1 satellites and will enhance the abilities of the GFM service.

Data availability. The dataset of this study is availble as Roth et al. (2022) at the TU Wien Research Data Repository. Generally, flood products to which the TU Wien flood mapping algorithm contributes to are available as part of the Global Flood Monitoring Service.

Author contributions. Conceptualization WW, BBM and FR; project supervision PS; statistics and validation FR; software MET and FR;
160 near-real-time processing CR; investigation FR; writing—original draft preparation FR; writing—review and editing ALL; visualisation BBM and FR; supervision BBM and WW; All authors have read and agreed to the published version of the manuscript. We like to thank the whole GFM consortium for their work on building a global flood mapping service.

Competing interests. The contact author has declared that none of the authors has any competing interests.

References

Bauer-Marschallinger, B., Cao, S., Tupas, M. E., Roth, F., Navacchi, C., Melzer, T., Freeman, V., and Wagner, W.: Satellite-Based Flood
170   Mapping through Bayesian Inference from a Sentinel-1 SAR Datacube, Remote Sensing, 14, 3673, 2022.

Gaurav, K., Sinha, R., and Panda, P.: The Indus flood of 2010 in Pakistan: a perspective analysis using remote sensing data, Natural hazards,
59, 1815–1826, 2011.

Global Flood Monitoring: GFM Product Definition Document, https://extwiki.eodc.eu/GFM/PDD/GFMoutputLayers#
output-layer-exclusion-mask, accessed: 2022-09-23.

175 Hoque, R., Nakayama, D., Matsuyama, H., and Matsumoto, J.: Flood monitoring, mapping and assessing capabilities using RADARSAT
remote sensing, GIS and ground data for Bangladesh, Natural Hazards, 57, 525–548, 2011.

Landuyt, L., Verhoest, N. E., and Van Coillie, F. M.: Flood mapping in vegetated areas using an unsupervised clustering approach on
Sentinel-1 and-2 imagery, Remote Sensing, 12, 3611, 2020.

NASA Earth Observatory: Devastating Floods in Pakistan, https://earthobservatory.nasa.gov/images/150279/devastating-floods-in-pakistan,
180   accessed: 2022-09-23.

Pekel, J.-F., Cottam, A., Gorelick, N., and Belward, A. S.: High-resolution mapping of global surface water and its long-term changes,
Nature, 540, 418–422, 2016.

Pelich, R., Chini, M., Hostache, R., Matgen, P., Delgado, J. M., and Sabatino, G.: Towards a global flood frequency map from SAR data, in:
2017 IEEE International Geoscience and Remote Sensing Symposium (IGARSS), pp. 4024–4027, IEEE, 2017.

185 Pierdicca, N., Pulvirenti, L., Boni, G., Squicciarino, G., and Chini, M.: Mapping flooded vegetation using COSMO-SkyMed: comparison
with polarimetric and optical data over rice fields, IEEE Journal of Selected Topics in Applied Earth Observations and Remote Sensing,
10, 2650–2662, 2017.

Qasim, S., Khan, A. N., Shrestha, R. P., and Qasim, M.: Risk perception of the people in the flood prone Khyber Pukhthunkhwa province of
Pakistan, International Journal of Disaster Risk Reduction, 14, 373–378, 2015.

190 Roth, F., Bauer-Marschallinger, B., Tupas, M. E., Reimer, C., Salamon, P., and Wagner, W.: Sentinel-1 based analysis of the Pakistan Flood
in 2022, https://doi.org/10.48436/zvvmh-nan78, 2022.

Roth, F., Tupas, M. E., Navacchi, C., Zhao, J., Wagner, W., and Bauer-Marschallinger, B.: Evaluation of a flood mapping algorithm based on
a Sentinel-1 datacube, ISPRS Journal of Photogrammetry and Remote Sensing, in preparation.

Sajjad, A., Lu, J., Chen, X., Chisenga, C., Saleem, N., and Hassan, H.: Operational monitoring and damage assessment of riverine flood-2014
195   in the lower Chenab plain, Punjab, Pakistan, using remote sensing and GIS techniques, Remote Sensing, 12, 714, 2020.

Salamon, P., Mctlormick, N., Reimer, C., Clarke, T., Bauer-Marschallinger, B., Wagner, W., Martinis, S., Chow, C., Böhnke, C., Matgen, P.,
et al.: The new, systematic global flood monitoring product of the copernicus emergency management service, in: 2021 IEEE International
Geoscience and Remote Sensing Symposium IGARSS, pp. 1053–1056, IEEE, 2021.

Sayama, T., Ozawa, G., Kawakami, T., Nabesaka, S., and Fukami, K.: Rainfall–runoff–inundation analysis of the 2010 Pakistan flood in the
200   Kabul River basin, Hydrological Sciences Journal, 57, 298–312, 2012.

Wang, Y.: Using Landsat 7 TM data acquired days after a flood event to delineate the maximum flood extent on a coastal floodplain,
International Journal of Remote Sensing, 25, 959–974, 2004.

Wania, A., Joubert-Boitat, I., Dottori, F., Kalas, M., and Salamon, P.: Increasing timeliness of satellite-based flood mapping using early
warning systems in the Copernicus Emergency Management Service, Remote Sensing, 13, 2114, 2021.